2007 IEEE International Conference on
Robotics and Automation
Roma, Italy, 10-14 April 2007

Active Strobe Imager for Visualizing Dynamic Behavior of Tumors

Makoto Kaneko, Chisashi Toya, and Masazumi Okajima

Abstract— **This paper newly proposes the Active Strobe Imager (ASI) that can visualize the dynamic behaviors of internal organ to medical doctors within Human dynamic eye sight, so that they can get a hint for detecting the location of tumors in real time during operation. The ASI is composed of a nozzle for supplying a pulsated air jet to an internal organ, a strobe system for visualizing the dynamic behaviors, a camera for capturing the image at the moment of strobe flashing, and a monitor for displaying the dynamic motion of internal organ, respectively. Without the assistance of strobe, medical doctors can not see what is really happening in real time, since the frequency of air jet is even more than the range of human dynamic eye sight. After explaining the basic principle, we show a couple of experiments for both artificial and real human lungs. Through these experiments, we newly found that the ASI is really helpful for discovering tumors or other diseases hidden in internal organs. Movies are available in website [1], [2].**

I. INTRODUCTION

Background: Suppose the Video Assisted Thoracic Surgery (VATS) as shown in Fig. 1(a), where a couple of small holes are opened in our side body and tumors in lung are removed by using both endoscope camera and forceps [3]-[6]. Before operation, the Computed Tomography (CT) can easily localize the position of tumors. By opening holes, however, the lung will shrink due to the change of pressure balance. In addition, medical doctors remove air from the lung so that they may acquire a surgery space. The shrinkage of lung will bring the shift of tumor position as shown in Fig. 1(b). Therefore, even if we carefully examine the location of tumors in advance by utilizing a CT, medical doctors are often obliged to look for them during operation. For a long time, it has been required to develop a sensing system capable of detecting the position of tumors during operation. The sensor should satisfy the following requirements: (i)The sensor should be slender enough to enable us to insert it in our body through a small hole opened, (ii)The sensor should work quick enough to enable us to utilize it in real time during operation, (iii)The image motion should be within the range of human dynamic eye sight. In our former work [7], we have developed the phase shift based impedance imager where the tumor is detected through the change of dynamic

M. Kaneko is with Graduate School of Engineering, Osaka University, 2-1, Yamadaoka, Suita, 565-0871, Japan (phone:81-6-6879-7331; fax:81-6-6879-4185; e-mail: mk@mech.eng.osaka-u.ac.jp).

C. Toya is with Graduate School of Engineering, Hiroshima University, 1-4-1, Kagamiyama, Higashi-hiroshima, 739-8527, Japan (phone:81-82-424-7690; fax:81-82-422-7158; e-mail: toya@hfl.hiroshima-u.ac.jp).

M. Okajima is with Graduate School of Biomedical Sciences, Hiroshima University Hospital, 1-2-3, Kasumi, Minami-ku, Hiroshima, 734-8551, Japan (phone:81-82-257-5222; fax:81-82-257-5224; e-mail: mokajima@hfl.hiroshima-u.ac.jp).

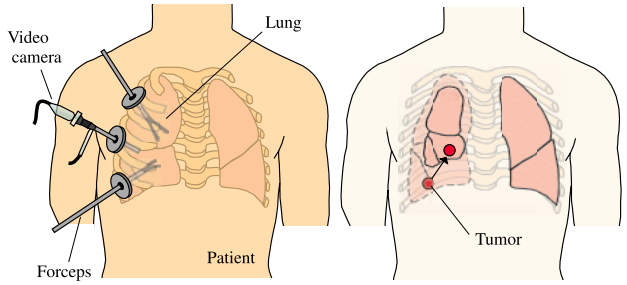

(a) Overview of VATS (b) Shift of tumor

Fig. 1. Video-Assisted Thoracic Surgery (VATS)

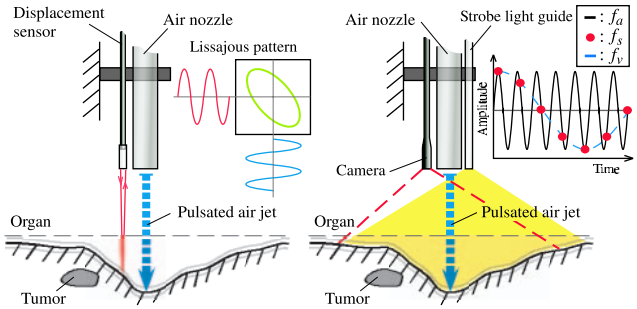

(a) Phase shift impedance imager (Local sensor)

(b) Active Strobe Imager (Global sensor)

Fig. 2. Local and global imagers

behavior of lung, when we scan the sensor over the surface of lungs by giving the pulsated air jet with the frequency of roughly 40[Hz]. The dynamic behavior of lung during the impartment of such a pulsated air jet is picked up by using an optical distance sensor implemented in parallel to an air nozzle with a proper distance, as shown in Fig. 2(a). The optical sensor can supply us with an output signal influenced by the distance up to the surface, the color of surface, and inclination of surface. In order to remove the influence of both color and inclination of surface, we focus on the phase difference of traveling wave between the force applying point and the position of optical sensor. Then, we can display the effect of tumor to medical doctors as a Lissajous pattern [8] as shown in Fig. 2(a). For human lungs in vitro, we have succeeded in showing a different Lissajous pattern over the surface where there exists a tumor. While we can see a successful result through the sensor, it can not provide us with a global information and, therefore, medical doctors can not judge in high reliability whether the phase shift really comes from tumors or not. On the other hand, when we observe the dynamic behavior by using a high speed

1-4244-0602-1/07/$20.00 ©2007 IEEE.

camera, we found that we can observe the dynamic behavior influenced by tumor even more clearly than the change of Lissajous pattern. The approach based on high speed camera, however, can not satisfy the requirement (ii), since we can see only through off line.

The goal of this work: We believe that the highest priority for medical diagnosis is to show medical doctors what is happening without any diagnosing software tool. This is because raw visual data should include rich information and a diagnosing software tool may eventually have a possibility for losing some important information. Our goal is to provide a new diagnosis system which can provide medical doctors with a dynamic behavior of internal organs in real time (requirement (ii)) and within human dynamic eye sight (requirement(iii)). If the frequency of air pulse is less than roughly 5[Hz], we can clearly observe how the deformation of lung is. On the other hand, under a high frequency such as 40[Hz], human can not see what is really happening by their naked eyes. This is due to the lack of dynamic eye sight of human. In order for medical doctors to be able to observe the dynamic behavior of lungs by naked eyes, we propose the Active Strobe Imager (ASI) composed of a nozzle for supplying a pulsated air jet to an internal organ, a strobe system for visualizing the dynamic behaviors, a camera for capturing the image at the moment of strobe flashing, and a monitor for displaying the dynamic motion of internal organ. Without the assistance of strobe, medical doctors can not see what is really happening in real time, since the frequency of air jet is even more than the range of human dynamic eye sight.

Organization of the paper: After briefly reviewing conventional works in chapter Ⅱ, the basic working principle of ASI is explained in chapter Ⅲ. Experimental results are shown in both artificial environment and human lungs in vitro in chapter Ⅳ. Through these experiments, we show that the ASI is really helpful for discovering tumors. In addition to this, we newly found that the ASI could discover diseases hidden in internal organs, while the conventional phase difference based approach could not. Finally, we give concluding remarks in chapter V.

II. Related Works

There have been a number of approaches for detecting tumors in our body. Basically, there are two approaches; one is the contact approach where a sensing probe directly makes contact with an organ and the other is the non-contact approach where a sensing probe never makes contact with an organ. One of most popular tools for contact approaches is perhaps a ultrasonic probe that can visualize internal organs as a density distribution [9]-[11]. This sensor often provides us with an important clue for examining whether there exists a tumor in our body or not. We would note, however, that the ultrasonic probe is not available for lungs, because voluminous air in lungs causes a strong attenuation for ultrasonic signal. The OLYMPUS Co., Ltd developed a proto type model which can estimate the location of a tumor through the impedance change before and after making contact with the environment [12]. While we can get pretty accurate information through the direct contact, the contact approach often causes damage to tissue due to the friction force and also may bring sanitary issue. These issues are not desirable, especially for medical applications. Furthermore, the contact approach produces invisible area during sensing, especially in the area where the probe makes contact with the tissue. Computed Tomography (CT) is an example of non-contact approaches. It can visualize the tumor existing in lungs through both multiple X-rays scanning [13]-[17]. Since it is not available in real time, unfortunately we can not use it for VATS. Also, receiving multiple X-rays is not good from the viewpoint of keeping patients' health. Kawahara and others have proposed the phase shift based non-contact impedance imager which can display the existence of tumor as a change of Lissajous pattern [7]. While this sensor can tell the phase shift information through the pattern to medical doctors in real time, they have to learn the know-how for understanding the meaning of the phase shift signal. Furthermore, the sensor can not obtain the area information without scanning motion. The Active Strobe Imager (ASI) proposed in this work try to solve these issues with keeping real time operation. As for strobe based medical diagnosis system, there is the Vocal Strobe Scope (VSS) capable of visualizing the vibration of vocal cord [18]-[20]. The idea of ASI is similar to that of VSS. The decisive difference point between two is that ASI includes the active force impartment mechanism, while the VSS does not. The active force impartment mechanism is not necessary for VSS, since the vocal cord can vibrate by itself. The mechanism is definitely necessary for internal organs except vocal cord, because they can not vibrate actively by themselves.

III. Active Strobe Imager (ASI)

A. Working Principle

Fig. 2(b) shows a conceptual image of ASI where it is composed of a nozzle for supplying pulsated air jet to an internal organ, a strobe system for visualizing the dynamic behaviors, a camera for capturing the image at the moment of strobe flashing, and a monitor for displaying the dynamic motion of internal organ. Fig. 2(b) shows two wave patterns where the real and the dotted lines are the air jet and the strobe flashing based waves, respectively. Let f_a, f_s, and F_h be the frequencies of air jet, strobe flashing, and the upper frequency where human can recognize in their dynamic eye sight, respectively. For example, under $f_a > F_h$, human can not see what is really happening, because the vibration is beyond their capability. In order for human to recognize what is happening by their naked eyes, we have to keep $f_a < F_h$ in general. We would note that there is a particular situation where we can observe the vibration through our naked eyes even under $f_a > F_h$, if we can rend the cyclic flashing by a strobe. Suppose f_s whose frequency is a bit smaller than f_a. Under such a situation, the real vibration with the

frequency of f_a can be shifted to a virtual vibration with the frequency $f_a - f_s$ where the "virtual vibration" means the vibration changed by the strobe flashing. Let us define the virtual frequency f_v where

$$f_v = |f_a - f_s| \tag{1}$$

If the following condition is satisfied, we can see the vibration by our naked eyes.

$$0 < f_v < F_h \tag{2}$$

With the assistance of strobe flashing in a dark environment, we can visualize the vibration produced by the pulsated air jet. This is the working principle of Active Strobe Imager (ASI). We would note that the ASI exhibits a great power especially for applying an internal organ when medical doctors try to find a tumor during operation. Of course, the strobe flashing is not necessary under $f_a < F_h$, since we can see the vibration directly. While the strobe flashing is only necessary under $F_h < f_a$, we would note that without a vibration with such a high frequency, it is hard to enhance the effect coming from tumors in diagnosing our internal organs.

B. Constraint condition on f_s

In this section, we explore the constraint conditions for choosing f_s by supposing $F_h < f_a$. The determination of f_a strongly depends upon the characteristics of the internal organs which we are interested in. In case of lungs, for example, it is known that f_a between 30[Hz] and 40[Hz] is appropriate for making the tumor in relief. When f_s is chosen close to f_a, we can obtain the virtual frequency f_v as shown in Fig. 2(b). In $f_s = f_a$, for example, the virtual frequency $f_v = 0$, which means that we can stop a virtual vibration and observe a particular phase only. By setting $f_s = f_a$ just after choosing a slightly different f_s from f_a, we can change the viewing point of wave step by step. Now, suppose that we set up the half strobe frequency for the one as shown in Fig. 2(b). In principle, we can observe the same virtual frequency even under such f_s, while the resolution of the wave is down. In general, there are a number of strobe frequencies leading to the same virtual frequency. Now, suppose that we choose an appropriate set of f_a and f_v satisfying in (2). Under this condition, (1) can be rewritten by

$$f_v = |f_a - nf_s| \tag{3}$$

where n is a natural number. Solving (3) with respect to f_s, we can obtain

$$f_s = \begin{cases} \frac{f_a - f_v}{n} & for \quad f_a - f_v > 0 \\ \frac{f_a + f_v}{n} & for \quad f_v - f_a > 0 \end{cases} \tag{4}$$

On the other hand, under an extremely large n, we gradually result in difficulty of recognizing the clear wave, and the lower boundary is given by

$$f_s > 2f_v \tag{5}$$

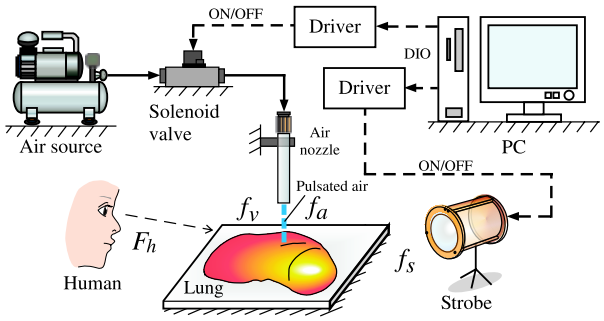

Fig. 3. Experimental setup

Eq. (5) is the well-known condition as Sampling Theorem for signal processing where a sampling frequency should be chosen two times larger than the maximum frequency of the original signal. As a result, a set of strobe frequency satisfying our requests is expressed by

$$f_s \in f_{s1} \cap f_{s2} \tag{6}$$

$$f_{s1} = \begin{cases} f_s : \frac{f_a - f_v}{n} & for \quad f_a - f_v > 0 \\ f_s : \frac{f_a + f_v}{n} & for \quad f_v - f_a > 0 \end{cases} \tag{7}$$

$$f_{s2} = f_s : f_s > 2f_v \tag{8}$$

IV. Experiments

A. Experimental System

Fig. 3 shows the experimental system where it is composed of a pulsated air supply system, an optical system and a computer for synchronously controlling both of them, respectively. The pulsated air supply system is further decomposed into a nozzle with its diameter of 3[mm] for providing a pulsated air, an air compressor for providing compressed air to the nozzle, and a solenoid valve for switching the air flow, respectively. The optical system is further decomposed into a strobe for supplying flashing light and a driver for controlling the frequency of flashing light, respectively. We can control the flashing frequency up to 400[Hz] and the switching frequency of valve up to 1[kHz], respectively. The PC sends the command signals to both the pulsated air supply system and the optical system. The pulsated air is generated in the following way.

$$f_a = \frac{1}{\tau_{on} + \tau_{off}}, \ (0 < f_a \leq 500[Hz]) \tag{9}$$

$$\alpha = \frac{\tau_{on}}{\tau_{on} + \tau_{off}}, \ (0 < \alpha \leq 1) \tag{10}$$

where τ_{on} and τ_{off} are time period for ON and OFF, respectively, and α is the duty factor for distributing the whole time period into ON and OFF, respectively. By giving both f_a and α, τ_{on} and τ_{off} are automatically determined.

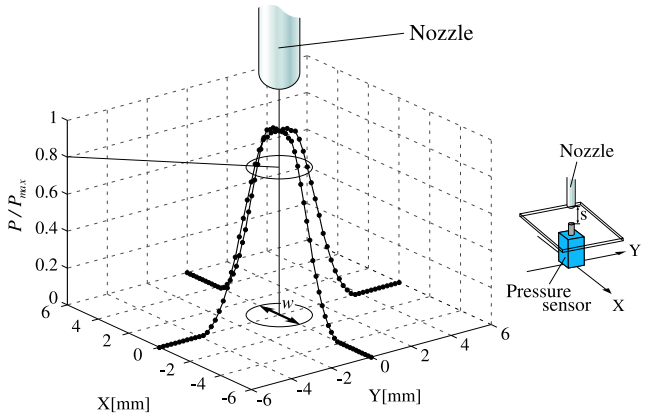

(a) Pressure distribution

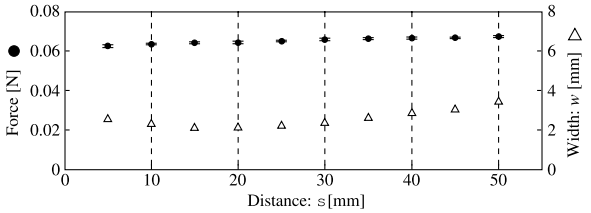

(b) Force with respect to distance

Fig. 4. Characteristics of air flow

B. Preliminary Experiments

Fig. 4(a) shows the pressure profile obtained under constantly supplied air flow, where the pressure distribution is measured by moving a pressure sensor in both X and Y directions step by step, respectively. The measured profile shows a pretty sharp profile where the width w at $P/P_{max} = 0.8$ is 2.3[mm] for the nozzle whose internal diameter is 3.0[mm]. Fig. 4(b) shows the generated force by changing the distance between the tip of nozzle and the environment, where "●" and "△" denote the force and the width at $P/P_{max} = 0.8$, respectively. The force is obtained by integrating the pressure with small area step by step. From Fig. 4(b), we can see that the applied force is almost constant while it slightly increases with respect to the distance. When the distance is extremely small, the air is blocked by the environment which avoids a natural flow due to the resistance. The effect may produce a smaller force as the distance is close to zero.

C. Experiments for Artificial Materials

$f_a = 35$[Hz] is given to the environment for all experiments. Fig. 5 shows the experimental results where (a), (b), (c), and (d) are for a uniform material under constant illumination ($f_s = 0$[Hz]), for a uniform material under $f_s = 34.5$[Hz], for the material with an artificial tumor in the depth of 5[mm] under $f_s = 34.5$[Hz], and for the material with an artificial tumor in the depth of 5[mm] under $f_s = 34.5$[Hz] respectively. While the experiments for both Fig. 5(c) and (d) are executed for the same environment, they have a different distance between the force applying point and the point with an artificial tumor, as shown in Fig. 5(c) and (d)

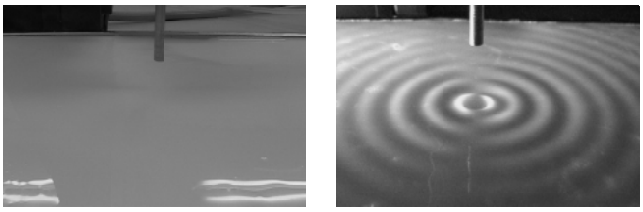

(a) $f_s = 0$[Hz] without any artificial tumor

(b) $f_s = 34.5$[Hz] without any artificial tumor

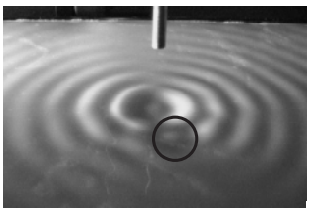

(c) $f_s = 34.5$[Hz] with an artificial tumor

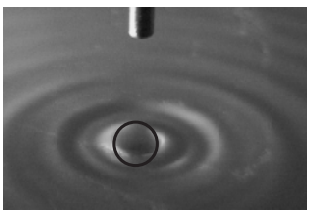

(d) $f_s = 34.5$[Hz] with on an artificial tumor at the point of mark ○

Fig. 5. Experimental results for artificial materials

where there exists an artificial tumor at the maker "○". From (1), $f_v = 0.5$[Hz] which surely satisfies the condition given by in (2). From Fig. 5(b) through (d), we can clearly observe the vibration of the surface of environment for the pulsated air jet, while we cannot see what is happening under $f_s = 0$[Hz]. An interesting observation is that the wave pattern in Fig. 5(c) is slightly different from that in Fig. 5(b). When the wave passes through the point where there exists the artificial tumor, the traveling speed locally changes, which brings unbalance wave pattern, as shown in Fig. 5(c). Another interesting point is that both Fig. 5(c) and (d) have also different wave patterns each other. The wave pattern varies depending upon where the force applying point is. Especially, when the force is given at the position where there exists the artificial tumor, the wave length is longer than that in other cases. A big advantage of ASI is that we can capture the existence of tumor through the global change of wave pattern in real time, which is hard for the conventional impedance sensors, such as phase shift based impedance imager [7].

D. Experiments for Human Lungs

We also challenge to apply the ASI for human lungs in vitro. Fig. 6 shows a removed lung where it includes normal tissue shown by the dotted circle A and emphysema shown by the dotted circle B. Emphysema is a disease where air vesicle is abnormally enlarged or multiple air vesicles are merged through the membrane breakage. We set $f_a = 40$[Hz] and $f_s = 39.5$[Hz], so that we can keep $f_v = 0.5$[Hz]. Fig. 7 and Fig. 8 show experimental results for normal part and for emphysema part, respectively. For normal part, we can see that the generated wave at the force applying point is transmitting toward the outer direction uniformly. The frequency of the wave is same as that of f_a. On the other hand, for emphysema part, we can observe an irregular wave pattern with different frequency from f_a in addition to a

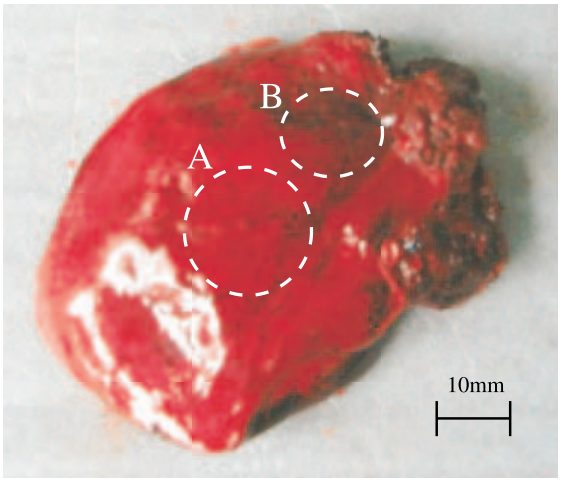

Fig. 6. An overview of removed human lung

similar wave pattern as that observed in normal part. Fig. 9 shows the frequency analysis for both experiments where (a) and (b) are normal and emphysema parts, respectively, and we purposely cut the waves whose frequencies are less than 0.5[Hz] so that we can enhance the wave whose frequency is more than the given frequency f_a. From Fig. 9, we can see that there exist various waves with different frequencies from f_a for emphysema part, while there is few waves with more than f_a for normal part. We would note that what is important is not to show the frequency analysis to medical doctors but to show what is happening as the real time visual image to medical doctors. Readers who are interested in seeing the movies of ASI, they are kindly requested to visit the website [1], [2].

V. Conclusions

We proposed a new non-contact active sensing system called Active Strobe Imager (ASI) which can show continuous visual image to medical doctors in real time. The sensor is composed of a nozzle for supplying a pulsated air jet to an internal organ, a strobe system for visualizing the dynamic behaviors, a camera for capturing the image at the moment of strobe flashing, and a monitor for displaying the dynamic motion of internal organ. Through experiments for human lungs, we showed that the emphysema can be enhanced by utilizing the ASI and medical doctors can easily detect it. Our next plan is to apply the ASI for animal lung in vivo.

Finally, this work was supported by the 21Century COE program, "Hyper Human Technology toward the 21 Century Industrial Revolution". We would express our gratitude for Dr. Tomohiro Kawahara for his strong assistance in both experiments and discussions. Also, we would express our sincere thanks to Medical Dr. Yoshihiro Miyata, Dr. Masanori Yoshimitsu, Dr. Koichi Akayama and Dr. Daisuke Sumitani for cooperation of this work.

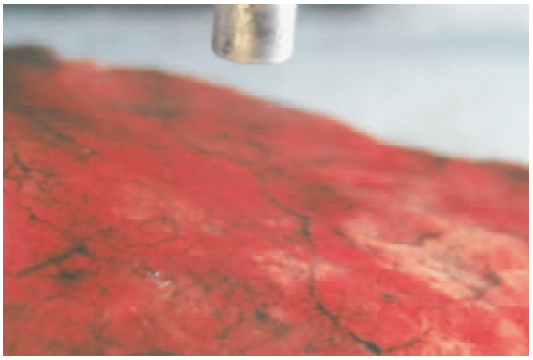

(a) Video image at $t = 0.00[s]$

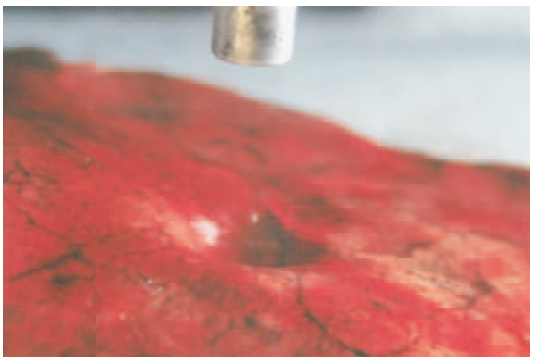

(b) Video image at $t = 6.16[s]$

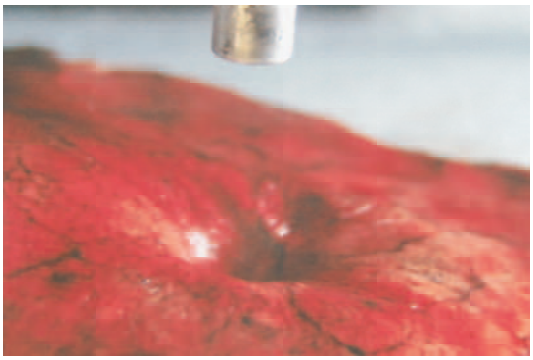

(c) Video image at $t = 8.44[s]$

Fig. 7. For a normal part of lung

References

[1] Movie of Fig.7.
Available: *http://www.hfl.hiroshima-u.ac.jp/˜toya/icra07/fig7.wmv*
[2] Movie of Fig.8.
Available: *http://www.hfl.hiroshima-u.ac.jp/˜toya/icra07/fig8.wmv*
[3] S. Kaseda, T. Aoki, N. Hangai, and K .Shimizu, "Better Pulmonary Function and Prognosis With Video-Assisted Thoracic Surgery Than With Thoracotomy", *Ann Thorac Surg*, vol. 70, pp. 1644-1646, 2000.
[4] D. A. Wakker, "Surgery for non-small cell lung cancer–new trends", *Lung Cancer*, vol. 34, pp. S133-S136, 2001.
[5] J. Lin, and M. D. Iannettoni, "The role of thoracoscopy in the management of lung cancer", *Surgical Oncology*, vol. 12, pp. 195-200, 2003.
[6] T. Nagayasu, "Video-Assisted Thoracic Surgery Lobectomy for Lung Cancer", *Acta Medica Nagasakiensia*, vol. 49, no. 3, pp. 75-79, 2004.
[7] T. Kawahara, C. Toya, N. Tanaka, M. Kaneko, Y. Miyata, M. Okajima, and T. Asahara, "Non-Contact Impedance Imager with Phase Differentiator", *Proc. of the 1st IEEE/RAS-EMBS Int. Conf. on Biomedical Robotics and Biomechatronics*, paper no 159, 2006.

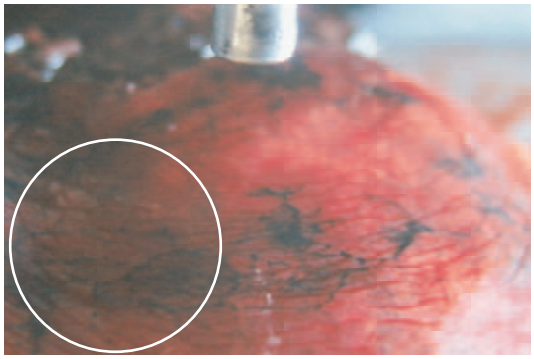

(a) Video image at $t = 0.00[s]$

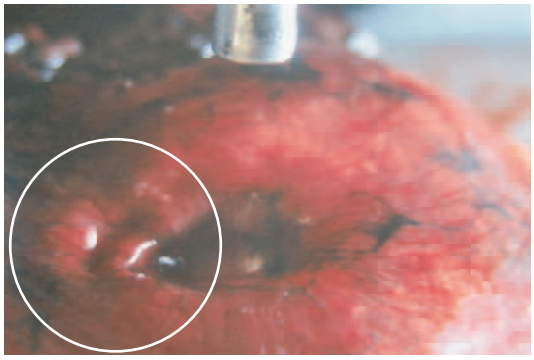

(b) Video image at $t = 2.07[s]$

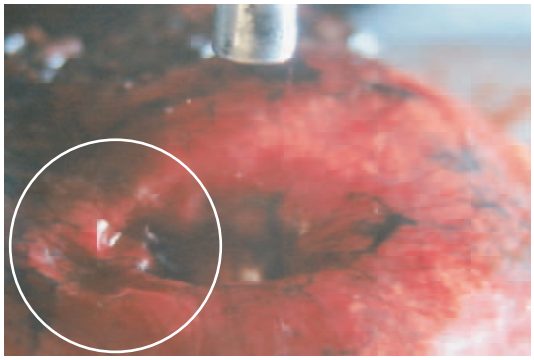

(c) Video image at $t = 7.13[s]$

Fig. 8. For a part of Pulmonary Emphysema

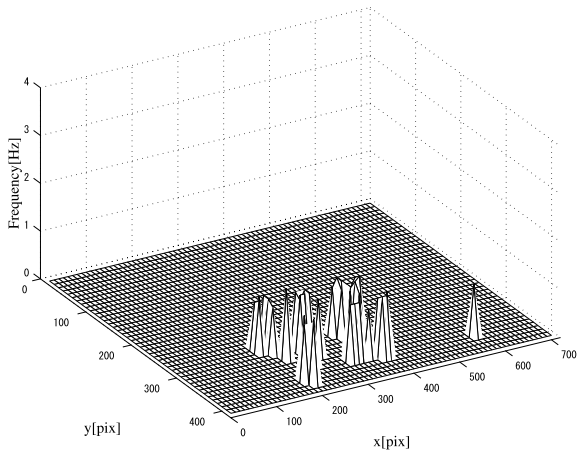

(a) Normal tissue of lung

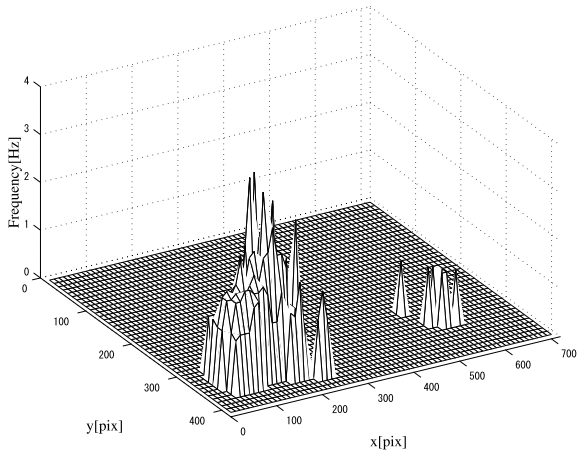

(b) Pulmonary emphysema of lung

Fig. 9. Frequency analysis

[8] Wolfram Math World.
Available: *http://mathworld.wolfram.com/LissajousCurve.html*

[9] O. Oshikawa, S. Tanaka, T. Ioka, A. Nakaizumi, Y. Hamada, and T. Mitani, "Dynamic Sonography of Pancreatic Tumors: Comparison with Dynamic CT", *American Journal of Roentgenology*, vol. 178, pp. 1133-1137, 2002.

[10] M. M. Moore, L. A. Whitney, L. Cerilli, J. Z. Imbrie, M. Bunch, V. B. Simpson, and J. B. Hanks, "Intraoperative Ultrasound Is Associated With Clear Lumpectomy Margins for Palpable Infiltrating Ductal Breast Cancer", *ANNALS OF SURGERY*, vol. 233, no. 6, pp. 761-768, 2001.

[11] TOSHIBA CORPORATION.
Available: *http://www.toshiba-iryouyouhin.co.jp/tmeds/*

[12] OLYMPUS CORPORATION.
Available: *http://www.olympus.co.jp/jp/lineup/index2.cfm*

[13] N. Lizza, P. Eucher, J. Haxhe, J. D. Wispelaere, P. M. Johnson, and L. Delaunois, "Thoracoscopic Recection of Pulmonary Nodules After Computed Tomographic-Guided Coil Labeling", *Ann Thorac Surg*, vol. 71, pp. 986-988, 2001.

[14] J. E. Husband, J. S. Macdonald, and M. J. Peckham, "Computed tomography in testicular disease: a review", *Journal of the Royal Society of Medicine*, vol. 74, pp. 441-447, 1981.

[15] M. A. Bredella, L. Steinbach, G. Caputo, G. Segall, R. Hawkins, "Value of FDG PET in the Assessment of Patients with Multiple Myeloma", *AJR*, vol. 184, pp. 1199-1204, 2005.

[16] D. Mcateer, F. Wallis, G. Couper, M. Norton, A. Welch, D. Bruce, K. Park, M. Nicolson, F. J. Gilbert, and P. Sharp, "Evaluation of (18)F-FDG positron emission tomography in gastric and oesophageal carcinoma", *The British Journal of Radiology*, vol. 72, pp. 525-529, 1999.

[17] J. H. Yim, P. Barton, B. Weber, D. Radford, J. Levy, B. Monsees, F. Flanagan, J. A. Norton, and G. M. Doherty, "Mammographically Detected Breast Cancer Benefits of Stereotactic Core Versus Wire Localization Biopsy", *ANNALS OF SURGERY*, vol. 223, no. 6, pp. 688-700, 1996.

[18] Laryngograph Ltd.
Available: *http://www.laryngograph.com/pr_lxstrobe.htm*

[19] N. Weir, and I. Bassett, "Outpatient fibreoptic nasolaryngoscopy and videostroboscopy", *Journal of the Royal Society of Medicine*, vol. 80, pp. 299-300, 1987.

[20] S. Saito, H. Fukuda, H. Ono, and Y. Isogai, "Observation of vocal fold vibration by x-ray stroboscopy", *The Journal of the Acoustical Society of America*, vol. 64, pp. S90-S91, 1978.